THE JOURNAL OF PHYSICAL CHEMISTRY C

Article

pubs.acs.org/JPCC

Translating XPS Measurement Procedure for Band Alignment into Reliable Ab Initio Calculation Method

Daoyu Zhang,*[,†] Minnan Yang,[‡] Huimin Gao,[†] and Shuai Dong*[,†]

[†]School of Physics, Southeast University, Nanjing 211189, China

[‡]Department of Physics, China Pharmaceutical University, Nanjing 211198, China

Supporting Information

ABSTRACT: Band alignment between solids is a crucial issue in condensed matter physics and electronic devices. Although the XPS method has been used as a routine method for determination of the band alignment, the theoretical calculations by copying the XPS band alignment procedure usually fail to match the measured results. In this work, a reliable ab initio calculation method for band alignment is proposed on the basis of the XPS procedure and in consideration of surface polarity and lattice deformation. Application of our method to anatase and rutile TiO_2 shows well agreement between calculation and experiment. Furthermore, our method can produce two types of band alignment: the coupled and the intrinsic, depending on whether the solid/solid interface effect is involved or not. The coupled and intrinsic band alignments correspond to alignments measured by XPS and electrochemical impedance analysis, respectively, explaining why band alignments reported by these two experiments are rather inconsistent.

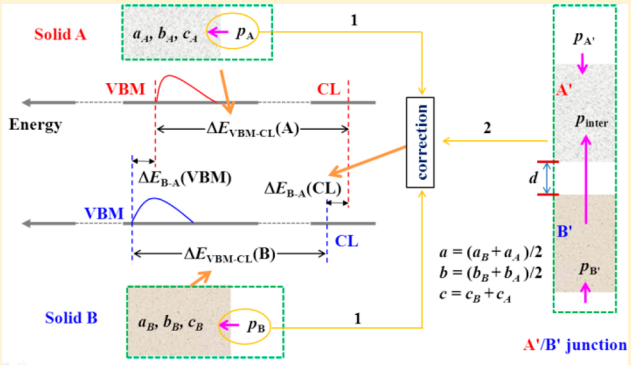

INTRODUCTION

The energy band alignment between solids is a fundamental concept in condensed matter physics and of crucial importance in design of electronic devices.[1−4] Many experimental methods, such as X-ray photoelectron spectroscopy (XPS), electrochemical impedance analysis (EIA), photoluminescence spectroscopy, surface photovoltage measurements, scanning probe microscopy, and so on, have been developed to measure the band alignment, the band offset, as well as the band bending. Among these methods, XPS is one of the most reliable and widely adopted choice.[5] Using XPS, the valence band offset between solids A and B, $\Delta E_{B\text{-}A}(VBM)$, can be expressed as follows:[6]

$$\Delta E_{B-A}(VBM) = [\Delta E_{VBM-CL}(B) - \Delta E_{VBM-CL}(A)] + \Delta E_{B-A}(CL) \quad (1)$$

where VBM stands for the valence band maximum and CL for the core level; $\Delta E_{Y-X}(Z)$ here and hereafter denotes the energy difference of level Z between systems Y and X, or the energy difference between levels Y and X in the system Z.

Unfortunately, directly employing eq 1 to calculate the band-offset using density functional theory (DFT) usually does not correctly reproduce the experimental values. For example, Wei et al. calculated the band offsets between all II−VI and III−V semiconductor compounds copying the XPS measurement procedure and found that some band offsets have large deviations from the experimental observations, especially between compounds with unavoidable lattice mismatch.[7] Chambers et al. studied the band offset at the epitaxial anatase TiO_2/n-$SrTiO_3$(001) interface, and their XPS measurement and DFT calculation showed bad agreement between theory and experiment.[8] Thus, they concluded that either DFT could not accurately calculate band offsets in the oxide materials, or some unknown factors (missed in the modeling) at the interface were influencing the band offset.

In fact, DFT is presently the most successful approach to compute the electronic structure of matter. Although the local density approximation (LDA) or generalized gradient approximation (GGA) will underestimate the correlation effects between electrons and the band gap, it remains anticipated to calculate band alignments between solids. Since the band alignment between solids is a relative energy value, the LDA or GGA error can be largely canceled in calculations.[9] For example, Ju et al. obtained the same band offsets between anatase and rutile TiO_2 by using the functional GGA and a more accurate hybrid exchange-correlation (XC) functional HSE06.[10] Therefore, the aforementioned failure of DFT prediction of band alignment should be due to other reasons.

AB INITIO BAND ALIGNMENT PROCEDURE

In this work, we attempt to translate the XPS measurement procedure for energy band alignment between solids to a

Received: January 27, 2017
Revised: March 9, 2017
Published: March 10, 2017

DOI: 10.1021/acs.jpcc.7b00900
J. Phys. Chem. C 2017, 121, 7139−7143

reliable ab initio calculation method. The effects from lattice mismatch and surface polarity are taken into account. The calculation procedure for the band alignment between solids A and B is illustrated in Figure 1. $\Delta E_{\text{VBM-CL}}(\text{A})$ and $\Delta E_{\text{VBM-CL}}(\text{B})$

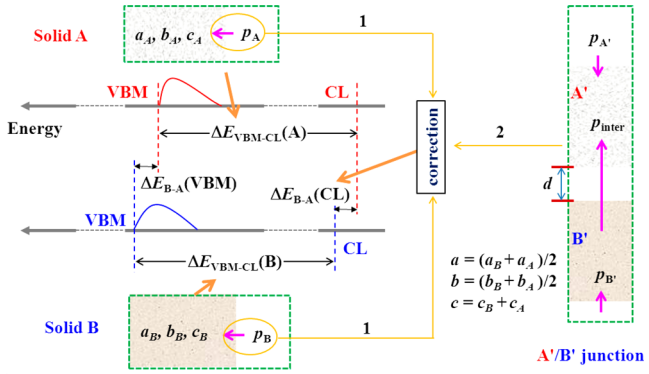

Figure 1. Schematic diagram of the procedure for calculating the band alignment between solids A and B, based on the XPS measurement procedure (eq 1). $\Delta E_{\text{VBM-CL}}(\text{A})$ and $\Delta E_{\text{VBM-CL}}(\text{B})$ can be calculated at their respective equilibrium lattice constants, while $\Delta E_{\text{B-A}}(\text{CL})$ can be obtained from the A′/B′ junction with corrections 1 and 2 (from the surface polarity and the expansion and/or compression of A and B respectively). The surface polarity, which is relative to the bulk one, is described by the electric dipole moment p. p_{inter} denotes the moment of the dipole layer induced by the interaction between two solids. The distance between two solids d can be tuned to change their interaction. When d is large enough, p_{inter} equals zero, and the band alignment between two solids is intrinsic; the nonzero p_{inter} will give a coupled band alignment.

terms in eq 1 can be calculated at their respective equilibrium lattice constants. The $\Delta E_{\text{B-A}}(\text{CL})$ term can be obtained from the unrelaxed A′/B′ heterojunction, but two corrections are needed for this term.

The first correction is from the surface polarity, which is introduced by the interruption of lattice periodicity. The polarity of an exposed surface may be represented by electric dipoles (moment p) perpendicular to the surface, as shown in Figure 2(a). Under the parallel-plate capacitor approximation the electrostatic potential difference (φ) between two sides of the capacitor can be expressed as follows:

$$\varphi = ep/(A\varepsilon_{\text{eff}}\varepsilon_0) \tag{2}$$

where e is the elementary charge; A is the surface area; ε_{eff} is the effective dielectric constant of the surface; and ε_0 is the permittivity of free space. If the average electrostatic potential of the system is taken as the energy reference, then the electrostatic potential created by the surface dipole layer increases the potential of ΔE^{VR} in the vacuum side of the capacitor and decreases the potential of ΔE^{SR} in the solid side. Figure 2(b) shows the superposition of this additional electrostatic potential from the surface dipole layer and the original electrostatic potential of the solid. The solid line in Figure 2(b) is the resulting electrostatic potential of the solid with an exposed surface. Thus, the surface polarity will lead to an increment of φ ($\varphi = \Delta E^{\text{VR}} - \Delta E^{\text{SR}}$) in the binding energy of every electron in the solid. In other words, the energy levels of both valence and core electrons in the solid will be shifted by the same amount of $-\varphi$ due to the surface polarity. The effect of surficial polarity on the energy levels might as well be put into

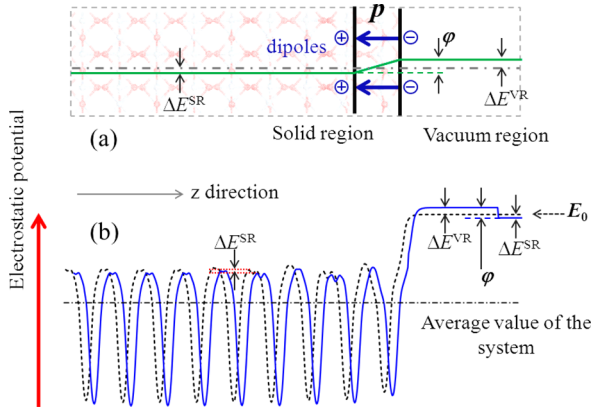

Figure 2. (a) The polarity surface of a solid and its polarity is represented by the electric dipole layer with the dipole moment of magnitude p. Under the parallel-plate capacitor approximation the electrostatic potential difference between the two plates is φ. If the average electrostatic potential of the system is taken as the energy reference, then the potential in the solid region decreases of ΔE^{SR} and that in the vacuum region increases of ΔE^{VR}. (b) Superposing the electrostatic potential of the surface dipole layer on the electrostatic potential of the solid, which is averaged in the xy plane parallel to the surface;[11] the dashed line indicates the potential without the surface dipoles.

the $\Delta E_{\text{B-A}}(\text{CL})$ term in eq 1, and the first correction is as follows:

$$\Delta E_{\text{B-A}}(\text{CL})_1 = [-\varphi(\text{B})] - [-\varphi(\text{A})] \tag{3}$$

The second correction comes from the lattice mismatch between solids when constructing the heterojunction. In theoretical calculations, the in-plane lattice should be expanded or compressed from original solids A and B to new A′ and B′ to form a junction supercell (see Figure 1). Thus, the core level difference between two solids calculated from the A′/B′ junction is $\Delta E_{\text{B′-A′}}(\text{CL})$, but evidently not the original $\Delta E_{\text{B-A}}(\text{CL})$.

The lattice deformation (i.e., the lattice expansion and/or compression) can lead to a change in the local atomic environment, and thus causes shifts of the core levels. For a given solid X and its deformed form X′, their core levels $cl(\text{X})$ and $cl(\text{X}')$ can be obtained from their respective ab initio calculations. Then the change of the core level from the lattice deformation can be determined by the following:

$$\begin{aligned}\Delta E_{\text{X′-X}}(\text{CL}) &= [cl(\text{X}') + \varepsilon_{\text{Fermi}}(\text{X}') - E_0(\text{X}')] \\ &\quad - [cl(\text{X}) + \varepsilon_{\text{Fermi}}(\text{X}) - E_0(\text{X})]\end{aligned} \tag{4}$$

where $\varepsilon_{\text{Fermi}}$ is the Fermi level, and E_0 is the vacuum level in the absence of surface polarity, as indicated in Figure 2(b). The method to determine $E_0(x)$ in ab initio calculations can be seen in the Supporting Information, SI.

Thus, the core level difference between solids A and B in the absence of surface polarity is as follows:

$$\begin{aligned}\Delta E_{\text{B-A}}(\text{CL}) &= \Delta E_{\text{B′-A′}}(\text{CL}) + [\Delta E_{\text{A′-A}}(\text{CL}) - \Delta E_{\text{B′-B}}(\text{CL})] \\ &= \Delta E_{\text{B′-A′}}(\text{CL}) + \Delta E_{\text{B-A}}(\text{CL})_2\end{aligned} \tag{5}$$

where $\Delta E_{\text{B-A}}(\text{CL})_2$ is the second correction for $\Delta E_{\text{B-A}}(\text{CL})$ due to lattice deformation.

By considering both eqs 3 and 5, finally the core level difference between solids A and B involving the surface polarity and the lattice deformation can be calculated as follows:

DOI: 10.1021/acs.jpcc.7b00900
J. Phys. Chem. C 2017, 121, 7139−7143

Table 1. Calculated Band Alignments between Rutile and Anatase TiO_2 with/without the Corrections[a,b,c,d]

		Ti 1*s*	Ti 2*s*	Ti 2*p*	O 1*s*	XPS	EIA*
$\Delta E_{VBM-CL}(R) - \Delta E_{VBM-CL}(A)$		-0.98	-0.94	-0.95	-0.98		
$\Delta E_{R'-A'}(CL)$	*a*	-3.81	-3.41	-3.46	-1.37		
	b	-3.54	-3.14	-3.19	-1.09		
$\Delta E_{R-A}(CL)_1$			0.26				
$\Delta E_{R-A}(CL)_2$		4.71	4.28	4.33	2.27		
$\Delta E_{R-A}(VBM)$	*a'*	-4.79	-4.35	-4.41	-2.35	0.39[30]	-0.04[A(101)[36]; R(110)[37]]
	a	0.18	0.19	0.18	0.18	0.7[38]	
	b'	-4.52	-4.08	-4.14	-2.07	0.37[39]	
	b	0.45	0.46	0.45	0.46		

[a]Values calculated using eq 7 when the distance *d* between two slabs R and A is 8.17 Å. *a'* Values calculated without corrections at *d* = 8.17 Å. [b]Values calculated using eq 7 at d = 1.67 Å. *b'* Values calculated without corrections at *d* = 1.67 Å. [c]Different core levels are adopted as the energy reference, which should not affect the final results of band alignment physically. Some corresponding experimental values taken from literature are also presented for reference. All energy values are in unit of eV. [d]The asterisk values in this column are calculated using eq S5.

$$\Delta E_{B-A}(CL) = \Delta E_{B'-A'}(CL) + \Delta E_{B-A}(CL)_1 + \Delta E_{B-A}(CL)_2 \quad (6)$$

Then the calculation method for the band alignment between two solids based on XPS measurement procedure is proposed as follows:

$$\Delta E_{B-A}(VBM) = [\Delta E_{VBM-CL}(B) - \Delta E_{VBM-CL}(A)] + \Delta E_{B'-A'}(CL) + \Delta E_{B-A}(CL)_1 + \Delta E_{B-A}(CL)_2 \quad (7)$$

However, the last two terms were usually missed in the previous band-alignment calculations based on XPS measurement.

It is worth noting that valence band alignment using eq 7 depends on the distance *d* between two solids in the junction supercell (see Figure 1). Therefore, two types of band alignment can be defined. When *d* is large enough to cancel the interaction between two solids, their band alignment is intrinsic. While the two solids approach closer, the interaction between them become stronger, e.g., the charges can transfer between them to induce the dipole layer at their interface. In such a case, the band alignment is called the coupled.

APPLICATION TO ANATASE AND RUTILE TiO_2

To illustrate the reliability of eq 7, the band alignment between anatase and rutile phase TiO_2 will be taken as an example. TiO_2 is the mostly studied metal oxide as a prototypical model system for heterogeneous catalysis,[12−16] photochemistry,[17−19] surface science,[20−23] and so on.[24−26] However, the band alignment of two phases of TiO_2 is an active and controversial topic.[27−33] The XPS experiments observed that the band-edge positions of rutile TiO_2 are higher than those of anatase, whereas EIA showed the band edges of anatase straddle those of rutile. The calculation method eq 7 proposed by us can explain this experimental discrepancy, as demonstrated below.

For real TiO_2 crystals, the anatase (101) and rutile (110) surfaces account for the majorities of exposed surfaces respectively, which will be adopted for the band alignment. These two surfaces are modeled by the stoichiometric $p(3 \times 1)$ rutile $TiO_2(110)$ and $p(1 \times 2)$ anatase $TiO_2(101)$ periodically repeated slabs with the vacuum space of ∼11 Å, respectively. All DFT+*U* calculations are performed using Vienna ab initio simulation package (VASP).[34,35] The core level energies are calculated under the initial state approximation. The corresponding core state eigenenergies are taken from any one of unfixed Ti or O near the center of the slabs. The detailed settings of calculation can be found in the SI.

The band alignments between anatase and rutile TiO_2 calculated by eq 7 are summarized in Table 1. For reference, some corresponding experimental observations are added into Table 1. In addition, the band alignments without the two corrections are also listed for comparison. Obviously, the $\Delta E_{R-A}(VBM)$ calculated without corrections exaggeratedly deviate from the experimental values, being no comparability with experimental values. Furthermore, it is physically unreasonable that the predicted values strongly depend on the selected core levels. In contrast, by taking the corrections implemented in eq 7, the predicted band offsets match the experimental ones very well. Besides, any selected core levels, e.g., Ti 1*s*, Ti 2*s*, Ti 2*p*, and O 1*s*, gives the identical values for band alignments in both the intrinsic and coupled conditions. This comparison implies that our proposed scenario for band alignment calculation (i.e., eq 7) is quite reliable.

The band alignment depends on the distance *d* between two surface slabs may be seen in Table 1 for our model of TiO_2 junction. The detailed distance-dependent value of the band alignment is shown in Figure 3. When the two surface slabs are separated by a vacuum space of more than 5 Å (corresponding to the weak interaction between them), their VBM offset approaches a constant, called by us the intrinsic band alignment. When *d* is less than 5 Å, the interaction between surface slabs is not negligible to the band offset. For example, when *d* is 1.67 Å, which is half the width of a trilayer of anatase (see Figure S2), the band offset is significantly different from the intrinsic value at *d* = 8.17 Å. The band alignment with the

DOI: 10.1021/acs.jpcc.7b00900
J. Phys. Chem. C 2017, 121, 7139−7143

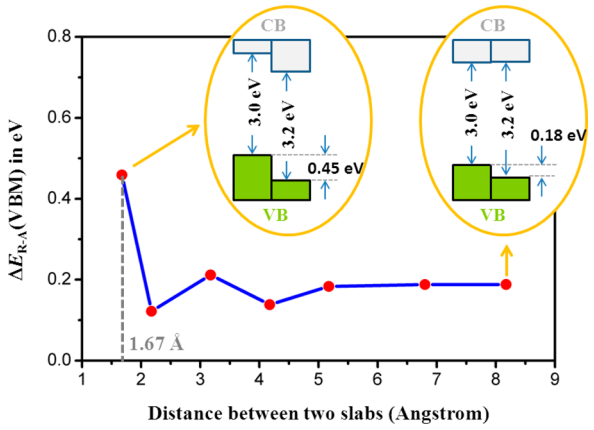

Figure 3. Band alignment between anatase and rutile TiO_2 varies as the distance d between two slabs.

strong solid/solid interface interaction was called by us the coupled one.

Besides the XPS method, the EIA method can also characterize the band alignment between two solids, which corresponds to the aforementioned intrinsic type because EIA separately measures the VBM or CBM positions of semiconductors. The principle of EIA measurement is briefly summarized in the SI. Our calculated intrinsic band alignment between two TiO_2 phases deviates somewhat from values of EIA measurements, which are listed in the last column of Table 1. This deviation may be caused by the surface adsorption of TiO_2 in the electrolyte solution and the compensation of surface polarity by adsorbates during the EIA measurements. Assuming the adsorbates on anatase (101) and rutile (110) surfaces completely compensate their surface polarity, the predicted $\Delta E_{R\text{-}A}$(VBM) should be −0.08 eV, very close to the EIA value of −0.04 eV.[36−39]

In contrast, the XPS measurement of the band alignment between two solids involves the solid/solid interface effect and thus corresponds to the coupled band alignment. Since the coupled band alignment is sensitive to the interfacial dipole layer which may be created by a change in the interfacial ions' configuration, charge transfer between two solids, etc., it is reasonable that the XPS experimental results of the band alignment between anatase and rutile TiO_2 are a little scattered. In fact, previous studies of the strain effect on the band structure of semiconductors had noticed that the change in interfacial atomic configuration, i.e., change of bond lengths, bond angles between interfacial atoms, does not lead to a much larger shift in VBMs of solids with an indeterminate sign:[40] the prolonged bond lengths decrease the bonding−antibonding splitting and the bandwidth, respectively increasing and decreasing the VBM energy, whereas, the shortened bond lengths behave inversely. In this sense, the band alignment calculated here without performing structural relaxation of the A′/B′ junction model to meet the elusive real interfacial atomic picture is a good approximation. Taking half the atomic periodicity of the longer-periodicity solid in the heterojunction along the z direction as the minimum value of d is reasonable to make overlapping of the atomic orbitals correct. Half the width of a trilayer of anatase (rutile) is 1.67 (1.59) Å (see Figure S2). Our calculated VBM band offset between anatase and rutile at d = 1.67 Å is 0.45 eV, which locates in the range of XPS values as expected (see Table 1). So, our coupled band alignment at the minimum value of d may act as a better approximation than the first approximation (the intrinsic band alignment) that commonly is used to help design of devices with solid interfaces.

CONCLUSIONS

In summary, an ab initio method for reliable calculation of band alignment between two solids has been proposed on the basis of the protocol of XPS measurement with two corrections in the core level from surface polarity and lattice deformation. Our method can yield two types of band alignment. The intrinsic band alignment free of the interfacial interaction between two solids corresponds to the band alignments measured by the EIA method, while the coupled one containing the interfacial interaction corresponds to the XPS measurement. The intrinsic and coupled band alignments between rutile and anatase TiO_2 calculated by our method are different but in good agreement with corresponding experimental observations. The theoretical principle of our work is independent of the type of material, and it may predict the band alignments between any two solids.

ASSOCIATED CONTENT

Supporting Information

The Supporting Information is available free of charge on the ACS Publications website at DOI: 10.1021/acs.jpcc.7b00900.

The method to determine E_0 methods and surface models and the band edge positions determined by EIA (PDF)

AUTHOR INFORMATION

Corresponding Authors

*E-mail: zhangdaoyu@seu.edu.cn (D.Z.).
*Tel./Fax: +86 25 52090606. E-mail: sdong@seu.edu.cn (S.D.).

ORCID

Daoyu Zhang: 0000-0003-3290-4410

Notes

The authors declare no competing financial interest.

ACKNOWLEDGMENTS

Work was supported by the National Natural Science Foundation of China (Grant No. 11674055).

REFERENCES

(1) Peressi, M.; Binggeli, N.; Baldereschi, A. Band Engineering at Interfaces: Theory and Numerical Experiments. *J. Phys. D: Appl. Phys.* **1998**, *31*, 1273−1299.
(2) Van de Walle, C. G.; Neugebauer, J. Universal Alignment of Hydrogen Levels in Semiconductors, Insulators and Solutions. *Nature* **2003**, *423*, 626−628.
(3) Walsh, A.; Butler, K. T. Prediction of Electron Energies in Metal Oxides. *Acc. Chem. Res.* **2014**, *47*, 364−372.
(4) Wei, S. H.; Zunger, A. Role of d-Orbitals in Valence-Band Offsets of Common-Anion Semiconductors. *Phys. Rev. Lett.* **1987**, *59*, 144−147.
(5) Zhang, Z.; Yates, J. T. Band Bending in Semiconductors: Chemical and Physical Consequences at Surfaces and Interfaces. *Chem. Rev.* **2012**, *112*, 5520−5551.
(6) Kraut, E. A.; Grant, R. W.; Waldrop, J. R.; Kowalczyk, S. P. Precise Determination of the Valence-Band Edge in X-Ray Photoemission Spectra - Application to Measurement of Semiconductor Interface Potentials. *Phys. Rev. Lett.* **1980**, *44*, 1620−1623.

DOI: 10.1021/acs.jpcc.7b00900
J. Phys. Chem. C 2017, 121, 7139−7143

(7) Wei, S. H.; Zunger, A. Predicted Band-Gap Pressure Coefficients of All Diamond and Zinc-Blende Semiconductors: Chemical Trends. *Phys. Rev. B: Condens. Matter Mater. Phys.* **1999**, *60*, 5404−5411.
(8) Chambers, S. A.; Ohsawa, T.; Wang, C. M.; Lyubinetsky, I.; Jaffe, J. E. Band Offsets at the Epitaxial Anatase TiO_2/N-$SrTiO_3$(001) Interface. *Surf. Sci.* **2009**, *603*, 771−780.
(9) Gai, Y. Q.; Li, J. B.; Li, S. S.; Xia, J. B.; Wei, S. H. Design of Narrow-Gap TiO(2): A Passivated Codoping Approach for Enhanced Photoelectrochemical Activity. *Phys. Rev. Lett.* **2009**, *102*, 036402.
(10) Ju, M.-G.; Sun, G.; Wang, J.; Meng, Q.; Liang, W. Origin of High Photocatalytic Properties in the Mixed-Phase TiO_2: A First-Principles Theoretical Study. *ACS Appl. Mater. Interfaces* **2014**, *6*, 12885−12892.
(11) Ma, X.; Dai, Y.; Yu, L.; Huang, B. Interface Schottky Barrier Engineering Via Strain in Metal-Semiconductor Composites. *Nanoscale* **2016**, *8*, 1352−1359.
(12) Babu, V. J.; Vempati, S.; Uyar, T.; Ramakrishna, S. Review of One-Dimensional and Two-Dimensional Nanostructured Materials for Hydrogen Generation. *Phys. Chem. Chem. Phys.* **2015**, *17*, 2960−2986.
(13) Chen, X.; Liu, L.; Huang, F. Black Titanium Dioxide (TiO_2) Nanomaterials. *Chem. Soc. Rev.* **2015**, *44*, 1861−1885.
(14) Li, J.; Wu, N. Semiconductor-Based Photocatalysts and Photoelectrochemical Cells for Solar Fuel Generation: A Review. *Catal. Sci. Technol.* **2015**, *5*, 1360−1384.
(15) Liu, B.; Zhao, X.; Terashima, C.; Fujishima, A.; Nakata, K. Thermodynamic and Kinetic Analysis of Heterogeneous Photocatalysis for Semiconductor Systems. *Phys. Chem. Chem. Phys.* **2014**, *16*, 8751−8760.
(16) Moniz, S. J. A.; Shevlin, S. A.; Martin, D. J.; Guo, Z.-X.; Tang, J. Visible-Light Driven Heterojunction Photocatalysts for Water Splitting - a Critical Review. *Energy Environ. Sci.* **2015**, *8*, 731−759.
(17) Kalyanasundaram, K. Photochemical Applications of Solar Energy: Photocatalysis and Photodecomposition of Water. In *Photochemistry: Vol. 41*; The Royal Society of Chemistry: London, 2013; Vol. *41*, pp 182−265.
(18) Wu, Z.; Zhang, W.; Xiong, F.; Yuan, Q.; Jin, Y.; Yang, J.; Huang, W. Active Hydrogen Species on TiO_2 for Photocatalytic H_2 Production. *Phys. Chem. Chem. Phys.* **2014**, *16*, 7051−7057.
(19) Zehr, R. T.; Henderson, M. A. Thermal Chemistry and Photochemistry of Hexafluoroacetone on Rutile TiO_2(110). *Phys. Chem. Chem. Phys.* **2010**, *12*, 8084−8092.
(20) Agosta, L.; Zollo, G.; Arcangeli, C.; Buonocore, F.; Gala, F.; Celino, M. Water Driven Adsorption of Amino Acids on the (101) Anatase TiO_2 Surface: An Ab Initio Study. *Phys. Chem. Chem. Phys.* **2015**, *17*, 1556−1561.
(21) Guo, Q.; Zhou, C.; Ma, Z.; Ren, Z.; Fan, H.; Yang, X. Elementary Photocatalytic Chemistry on TiO_2 Surfaces. *Chem. Soc. Rev.* **2016**, *45*, 3701−3730.
(22) Lun Pang, C.; Lindsay, R.; Thornton, G. Chemical Reactions on Rutile TiO_2(110). *Chem. Soc. Rev.* **2008**, *37*, 2328−2353.
(23) Zhang, D. Y.; Yang, M. N.; Dong, S. Improving the Photocatalytic Activity of TiO_2 through Reduction. *RSC Adv.* **2015**, *5*, 35661−35666.
(24) Li, H. F.; Yu, H. T.; Quan, X.; Chen, S.; Zhao, H. M. Improved Photocatalytic Performance of Heterojunction by Controlling the Contact Facet: High Electron Transfer Capacity between TiO_2 and the {110} Facet of $BiVO_4$ Caused by Suitable Energy Band Alignment. *Adv. Funct. Mater.* **2015**, *25*, 3074−3080.
(25) Zhang, D. Y.; Yang, M. N. Band Structure Engineering of TiO_2 Nanowires by N-P Codoping for Enhanced Visible-Light Photoelectrochemical Water-Splitting. *Phys. Chem. Chem. Phys.* **2013**, *15*, 18523−18529.
(26) Zhang, Y.; Jiang, Z.; Huang, J.; Lim, L. Y.; Li, W.; Deng, J.; Gong, D.; Tang, Y.; Lai, Y.; Chen, Z. Titanate and Titania Nanostructured Materials for Environmental and Energy Applications: A Review. *RSC Adv.* **2015**, *5*, 79479−79510.
(27) Kullgren, J.; Aradi, B.; Frauenheim, T.; Kavan, L.; Deak, P. Resolving the Controversy About the Band Alignment between Rutile and Anatase: The Role of OH^-/H^+ Adsorption. *J. Phys. Chem. C* **2015**, *119*, 21952−21958.
(28) Mi, Y.; Weng, Y. Band Alignment and Controllable Electron Migration between Rutile and Anatase TiO_2. *Sci. Rep.* **2015**, *5*, 11482−11482.
(29) Nosaka, Y.; Nosaka, A. Y. Reconsideration of Intrinsic Band Alignments within Anatase and Rutile TiO_2. *J. Phys. Chem. Lett.* **2016**, *7*, 431−434.
(30) Scanlon, D. O.; Dunnill, C. W.; Buckeridge, J.; Shevlin, S. A.; Logsdail, A. J.; Woodley, S. M.; Catlow, C. R. A.; Powell, M. J.; Palgrave, R. G.; Parkin, I. P.; et al. Band Alignment of Rutile and Anatase TiO_2. *Nat. Mater.* **2013**, *12*, 798−801.
(31) Zhang, D. Y.; Yang, M. N.; Dong, S. Electric-Dipole Effect of Defects on the Energy Band Alignment of Rutile and Anatase TiO_2. *Phys. Chem. Chem. Phys.* **2015**, *17*, 29079−29084.
(32) Deak, P.; Aradi, B.; Frauenheim, T. Band Lineup and Charge Carrier Separation in Mixed Rutile-Anatase Systems. *J. Phys. Chem. C* **2011**, *115*, 3443−3446.
(33) Wang, C.; Zhang, X.; Wei, Y.; Kong, L.; Chang, F.; Zheng, H.; Wu, L.; Zhi, J.; Liu, Y. Correlation between Band Alignment and Enhanced Photocatalysis: A Case Study with Anatase/ TiO_2(B) Nanotube Heterojunction. *Dalton Trans.* **2015**, *44*, 13331−13339.
(34) Blochl, P. E. Projector Augmented-Wave Method. *Phys. Rev. B: Condens. Matter Mater. Phys.* **1994**, *50*, 17953−17979.
(35) Kresse, G.; Furthmuller, J. Efficient Iterative Schemes for Ab Initio Total-Energy Calculations Using a Plane-Wave Basis Set. *Phys. Rev. B: Condens. Matter Mater. Phys.* **1996**, *54*, 11169−11186.
(36) Kavan, L.; Gratzel, M.; Gilbert, S. E.; Klemenz, C.; Scheel, H. J. Electrochemical and Photoelectrochemical Investigation of Single-Crystal Anatase. *J. Am. Chem. Soc.* **1996**, *118*, 6716−6723.
(37) Nakamura, R.; Ohashi, N.; Imanishi, A.; Osawa, T.; Matsumoto, Y.; Koinuma, H.; Nakato, Y. Crystal-Face Dependences of Surface Band Edges and Hole Reactivity, Revealed by Preparation of Essentially Atomically Smooth and Stable (110) and (100) N-TiO_2 (Rutile) Surfaces. *J. Phys. Chem. B* **2005**, *109*, 1648−1651.
(38) Pfeifer, V.; Erhart, P.; Li, S.; Rachut, K.; Morasch, J.; Broetz, J.; Reckers, P.; Mayer, T.; Ruehle, S.; Zaban, A.; et al. Energy Band Alignment between Anatase and Rutile TiO_2. *J. Phys. Chem. Lett.* **2013**, *4*, 4182−4187.
(39) Xiong, G.; Shao, R.; Droubay, T. C.; Joly, A. G.; Beck, K. M.; Chambers, S. A.; Hess, W. P. Photoemission Electron Microscopy of TiO_2 Anatase Films Embedded with Rutile Nanocrystals. *Adv. Funct. Mater.* **2007**, *17*, 2133−2138.
(40) Li, Y. H.; Gong, X. G.; Wei, S. H. Ab Initio Calculation of Hydrostatic Absolute Deformation Potential of Semiconductors. *Appl. Phys. Lett.* **2006**, *88*, 042104.

DOI: 10.1021/acs.jpcc.7b00900
J. Phys. Chem. C 2017, 121, 7139−7143